Supplement of Atmos. Chem. Phys., 21, 2569–2583, 2021
https://doi.org/10.5194/acp-21-2569-2021-supplement

Atmospheric Chemistry and Physics
Open Access
EGU

Supplement of

Measurement report: Distinct emissions and volatility distribution of intermediate-volatility organic compounds from on-road Chinese gasoline vehicles: implication of high secondary organic aerosol formation potential

Rongzhi Tang et al.

Correspondence to: Song Guo (songguo@pku.edu.cn) and Allen L. Robinson (alr@andrew.cmu.edu)

S1 Description of the experimental procedures

The measurements were performed on a Chinese in-use gasoline vehicle recruited from a rental car agency in Beijing in August-September, 2018. All the tests were conducted using the vehicle chassis dynamometer at the State Key Laboratory of Automotive Safety and Energy at Tsinghua University. Test cycled included a specially designed CLTC cycle based on Chinese real-world road condition and a widely used world-wide unified cycle called World-wide harmonized Light duty Test Cycle (WLTC). WLTC was designed to harmonize driving cycle from "real world" driving data in different regions around world i.e. Europe, India, Japan, Korea and USA, combined with suitable weighting factors(Tutuianu et al., 2015). There are four speed classes in WLTC cycle: low, medium, high and extra-high speed phases, which can cover different road types (urban, rural, motorway) and driving conditions (peak, off-peak, weekend). To better investigate the real emissions of IVOCs in China, a specially designed cycle called CLTC was applied in this study. It was developed to represent real driving condition in megacities (like Beijing) of China. In total, it has three velocity stages, namely low, medium and high-speed phases. The total duration time for the two cycles was 1800 seconds. Previous studies found that cold- versus hot-start can also have an influence on the IVOC emission. Therefore, hot-start and cold-start system were both used in the tested CLTC and WLTC to evaluate the IVOC emission effects. Apart for this, specially designed acceleration rate cycles were also applied in this study to assess the reasons for the differences occurred during CLTC and WLTC cycle.

S2 Quantification and qualification of specified IVOCs

IVOCs collected by the adsorption tube filled with Tenax TA were thermally desorbed using Gerstel thermal desorption module (TDS3) followed by pre-concentration using a Gerstel cooled injection system (CIS4). The CIS4 was then heated to 300 ^{o}C by programming heating and transported the organic precursors to the GC/MS for analysis. Prior to analysis, a known amount of deuterated standards including d8-naphthalene and C12, C16, C20, C24, C30, C32, C36 deuterated n-alkanes were injected into the adsorption tube to track IVOC recovery during analysis. Concentrations of individual IVOCs were quantified using calibration curves developed by injecting a series of known amount of standard solutions into preconditioned clean tubes. The calibration standards include C8-C40 n-alkane and some aromatics, the results were listed in Table S1.

S3 Quantification of unspeciated IVOCs

Unspeciated IVOCs, which we call as IVOC UCMs, could not be fully characterized by GC-MS. To quantify the total IVOC concentration, we used the total ion current (TIC) signal from the chromatography following the approach of Zhao et al. (2016). The TIC was divided into 11 bins based on the n-alkanes retention time (equivalent as the volatility). The IVOC UCM were classified as unspeciated b-alkanes and unspeciated cyclic compounds following Zhao et al. (2016). The IVOCs were then categorized into each bins corresponding to the n-alkane (Cn) where n represents the carbon number of n-alkane, called Bn.

The time range of the Bn bins could be calculated using the following method,

$$t_{n,binstart} = t_n - \frac{t_n - t_{n-1}}{2} \quad (1)$$

$$t_{n,binend} = t_n + \frac{t_{n+1} - t_n}{2} \quad (2)$$

In the above equations, t_n is the retention time of the n-alkane, while t_{n-1} and t_{n+1} stand for the retention time of the C_{n-1} and C_{n+1} n-alkanes.

The IVOC mass in each bin was calculated using the mass/signal response of the C_n n-alkane in the same bin, which could be described as follows:

$$M_{IVOCs,Bn} = \frac{TA_{TIC,Bn}}{RF_{n-alkane,Cn}} = \frac{TA_{m/z57,Bn}}{RF_{n-alkane,Cn}} \times \frac{1}{f_{m/z57,TIC\_Bn}} \quad (3)$$

$TA_{TIC,Bn}$ means the TIC abundance in the Bn bin, $RF_{n\text{-}alkane,Cn}$ is the response factor for n-alkane (Cn); $TA_{mz/57,Bn}$ respresents the m/z57 abundance in Bn bin, while $f_{m/z,57,TIC,Bn}$ denotes the fraction of m/z 57 to TIC in the Bn bin. The IVOC UCM_{Bn} was determined as the total IVOC minus the speciated IVOC in each Bn bin.

The mass of b-alkanes in each Bn bin was calculated as:

$$M_{b-alkane,Bn} = \frac{BA_{b-alkane,Bn}}{RF_{n-alkane,Cn}} = \frac{BA_{m/z57,Bn}}{RF_{n-alkane,Cn}} \times \frac{1}{f_{m/_{z57},b-alkane\_Bn}} = \frac{TA_{m/z57,Bn} - NA_{m/z57,Bn}}{RF_{n-alkane,Cn}} \times \frac{1}{f_{m/_{z57},b-alkane\_Bn}} \quad (4)$$

In this equation, $BA_{b\text{-}alkane,Bn}$ denotes the abundance of *b*-alkane in the Bn bin, $BA_{m/z57,Bn}$ represents the m/57 abundance derived from b-alkane in Bn bin, while $TA_{m/z57,Bn}$ is the total m/z57 signal in Bn bin. $NA_{m/z57,Bn}$ is the m/z 57 abundance produced by n-alkanes; $f_{m/z57,b\text{-}alkane\_Bn}$ means the m/z57 fraction of the TIC for b-alkanes.

Based on the calculation above, we determine the mass of the unspeciated cyclic compounds.

S5 Uncertainty of IVOCs measurement

The uncertainty of the IVOCs could be ascribed to both sampling and analysis. When sampling, the positive/negative adsorption/desorption of the target compounds on quartz filters/Tenax tubes (May et al., 2013) and slight flow fluctuation will cause sampling uncertainty which we assume a value of 10% (Huang et al., 2019). The uncertainty of using *n*-alkanes as surrogate standards for the total IVOC mass was estimated to be less than 6.0% for alkanes and 30.6% for PAHs based on the analysis of a suite of standard compounds (Table S4). The overall uncertainty for IVOCs measurement was determined to be 32.2% according to error propagation.

$$\mathrm{UNC}_{\mathrm{IVOCs}} = \sqrt{(\sigma^2_{\mathrm{sampling}} + \sigma^2_{\mathrm{measurement}})} \quad (5)$$

S4 Comparison between China V and LEV-2 vehicles

IVOCs and VOCs are both subgroups of THC, so higher contribution of IVOC to THC reduces the VOC-to-THC ratio. Using the same set of 65 VOCs measured by both the US and Chinese tests, the median VOC-to-THC ratios for China V and US vehicle were 0.36 and 0.46, respectively (Figure S7). Comparison of VOCs emissions by chemical compositions can be found in Figure S8. For most of the speciated VOC/THC ratio, China V was lower than that of the LEV-2, except for benzene and C7-C11 n-alkanes where China V has higher values. This might suggest a shift of emissions to low volatility range happen to China V vehicles.

Supplemental Figures

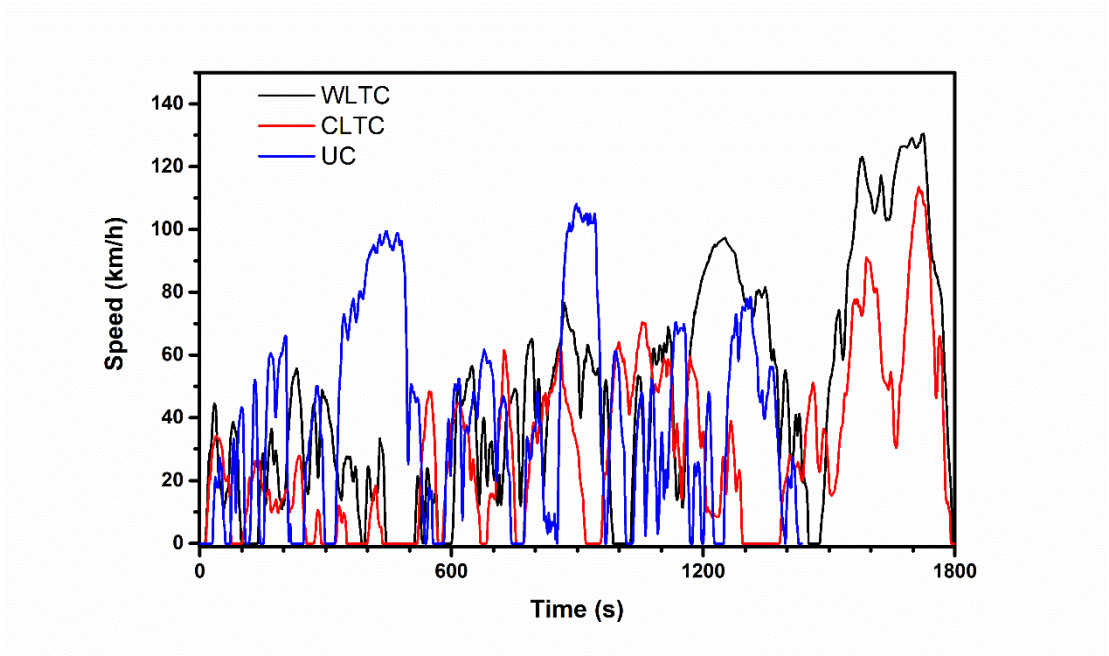

Figure S1. Speed profiles of WLTC, CLTC and UC protocols

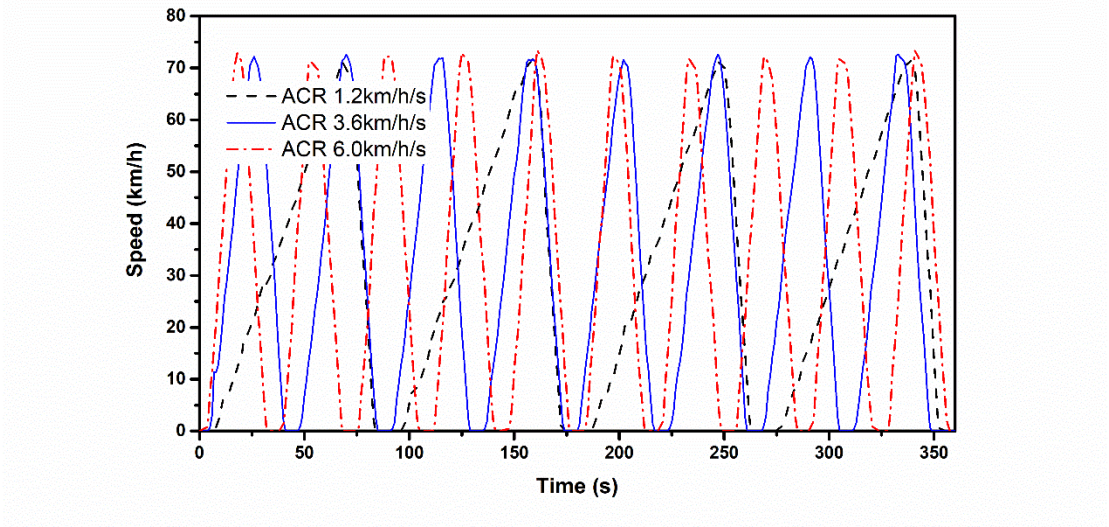

Figure S2. Specific designed cycles at different acceleration rates.

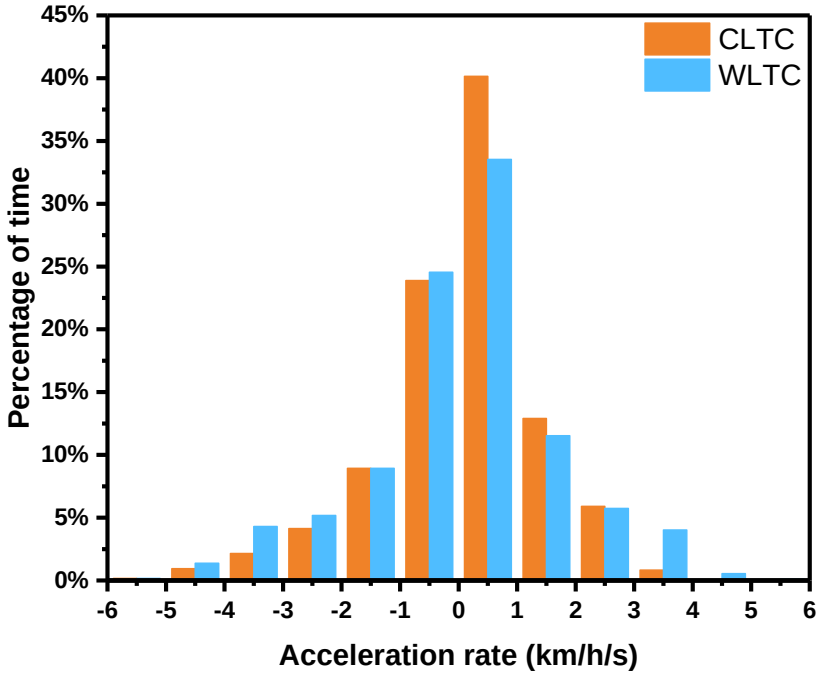

Figure S3. Histogram distribution of acceleration rate for WLTC and CLTC

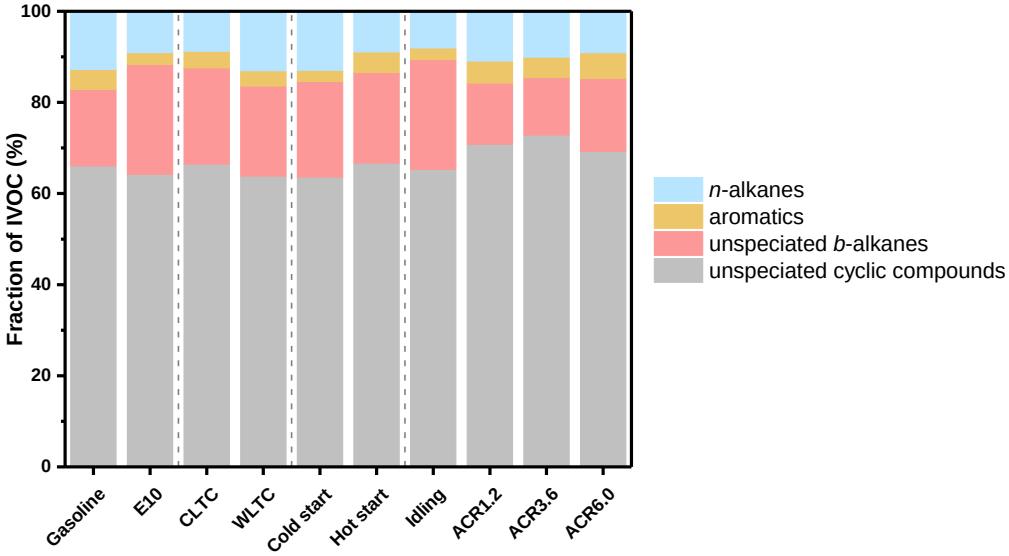

Figure S4. Comparison of IVOC fraction under different operating conditions, here the aromatics represent the PAHs listed in Table S4.

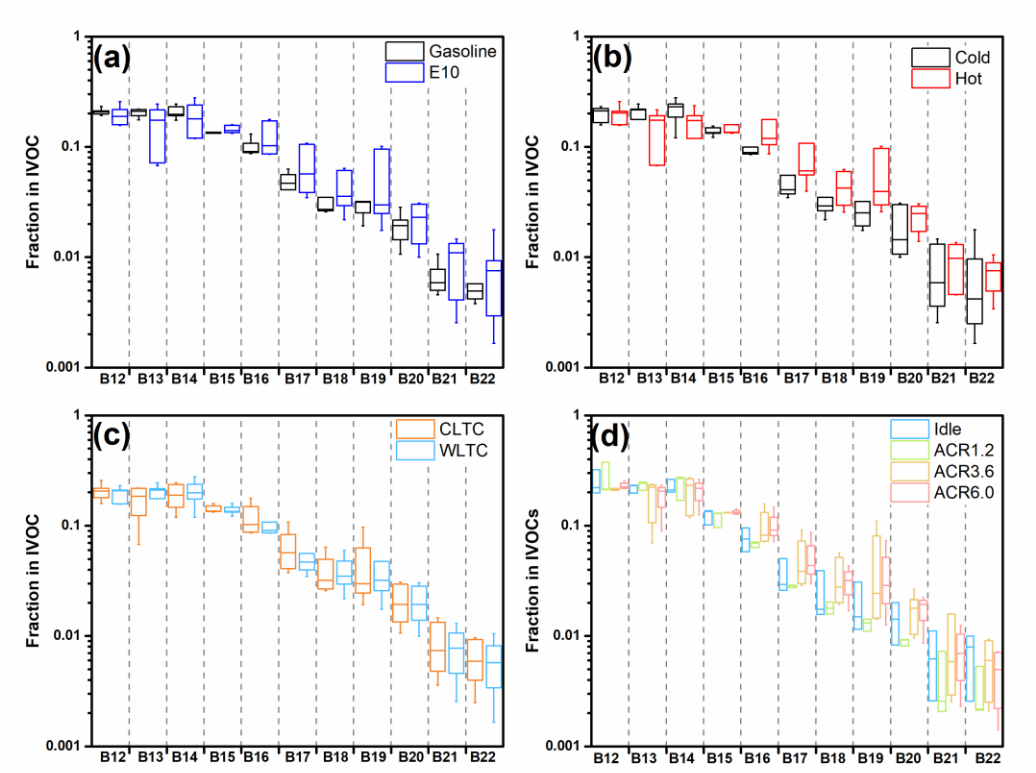

Figure S5. IVOC volatility distributions under different operations:(a) fuel; (b) starting mode; (c) operating cycle; (d) acceleration rates. The boxes represent the 75th and 25th percentiles, with the centerline being the median. The whiskers are the highest and lowest values.

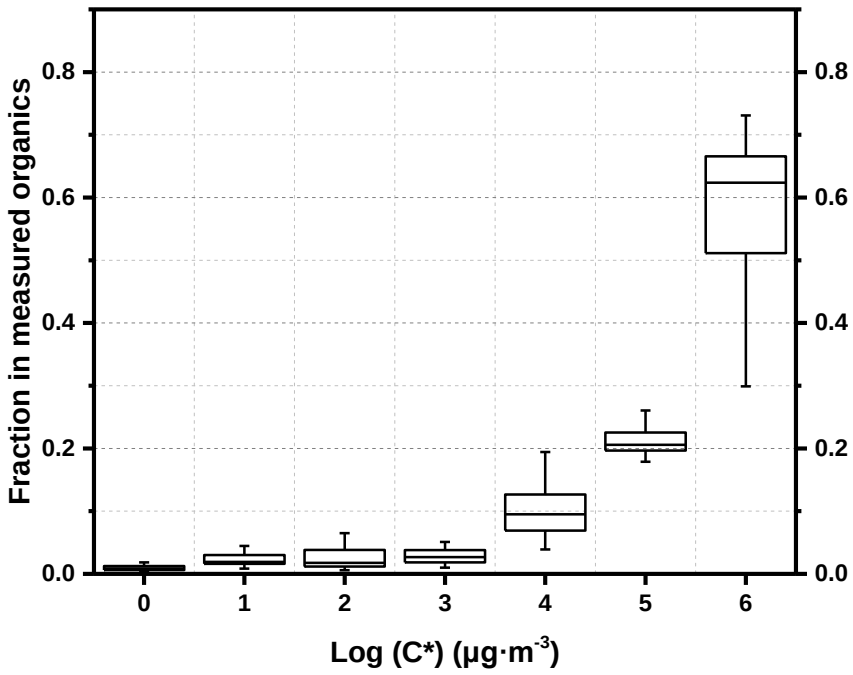

Figure S6. Volatility distribution of organics measured by GC/MS of adsorbent tubes collected during all the tests for the tested China V gasoline vehicle. The boxes represent the 75th and 25th percentiles, with the centerline being the median. The whiskers are the highest and lowest values.

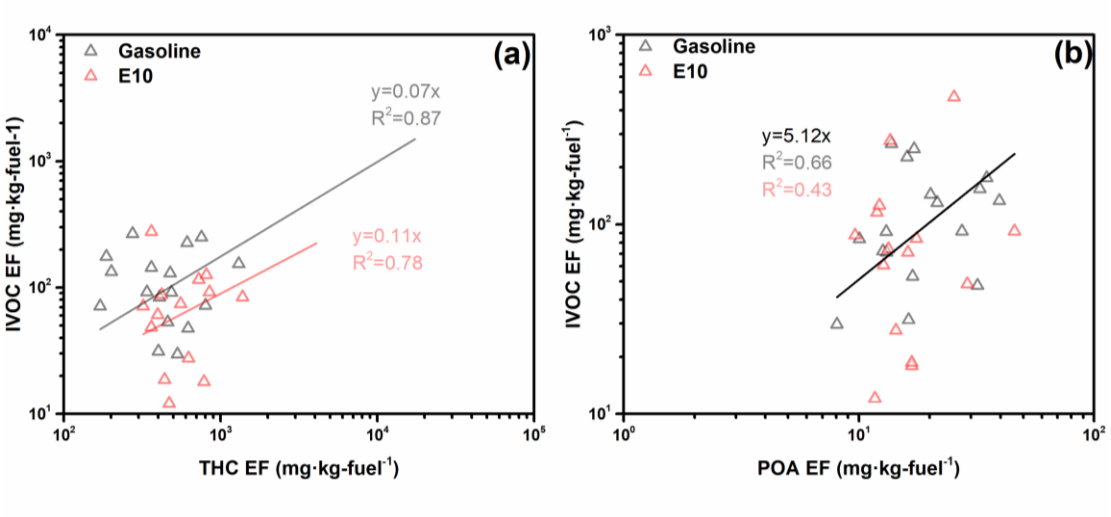

Figure S7. Scatter plots of IVOC EFs and (a) THC EFs and (b) POA EFs from the tested gasoline vehicle under different operating conditions. The gray triangles represent data obtained using gasoline as the fuel. The light red triangles stand for data taken when the gasoline vehicle was fueled with E10.

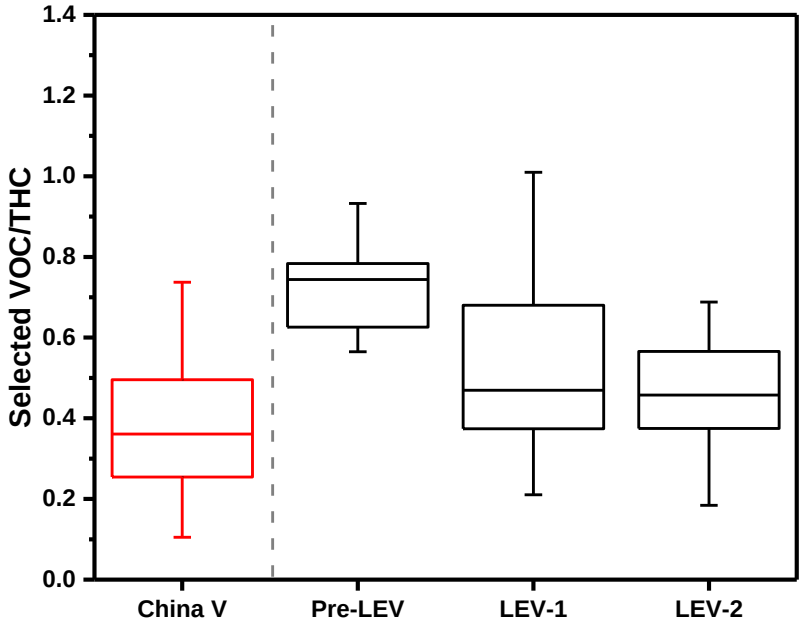

Figure S8. Comparison of selected VOC/THC between China V and US vehicles in different model years. Selected VOC means restrained 65 VOC species which both measured in China V and US vehicles.

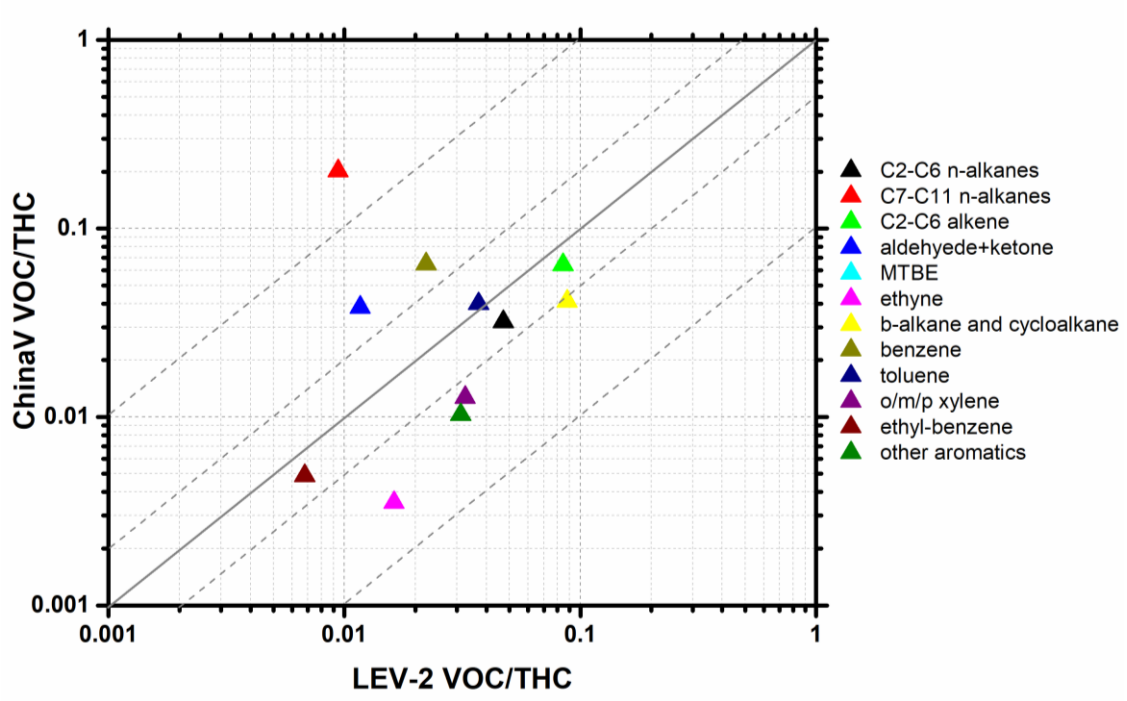

Figure S9. Comparison of VOC/THC between China V and LEV-2, grouped by VOC composition.

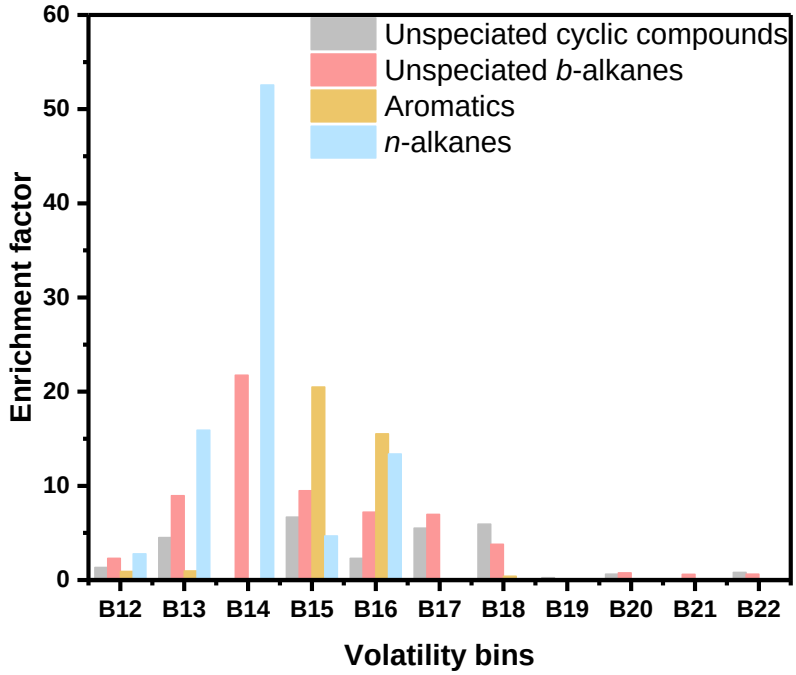

Figure S10. Median enrichment mass fraction (exhaust vs fuel) grouped by volatility bins, indicating the composition change after combustion process.

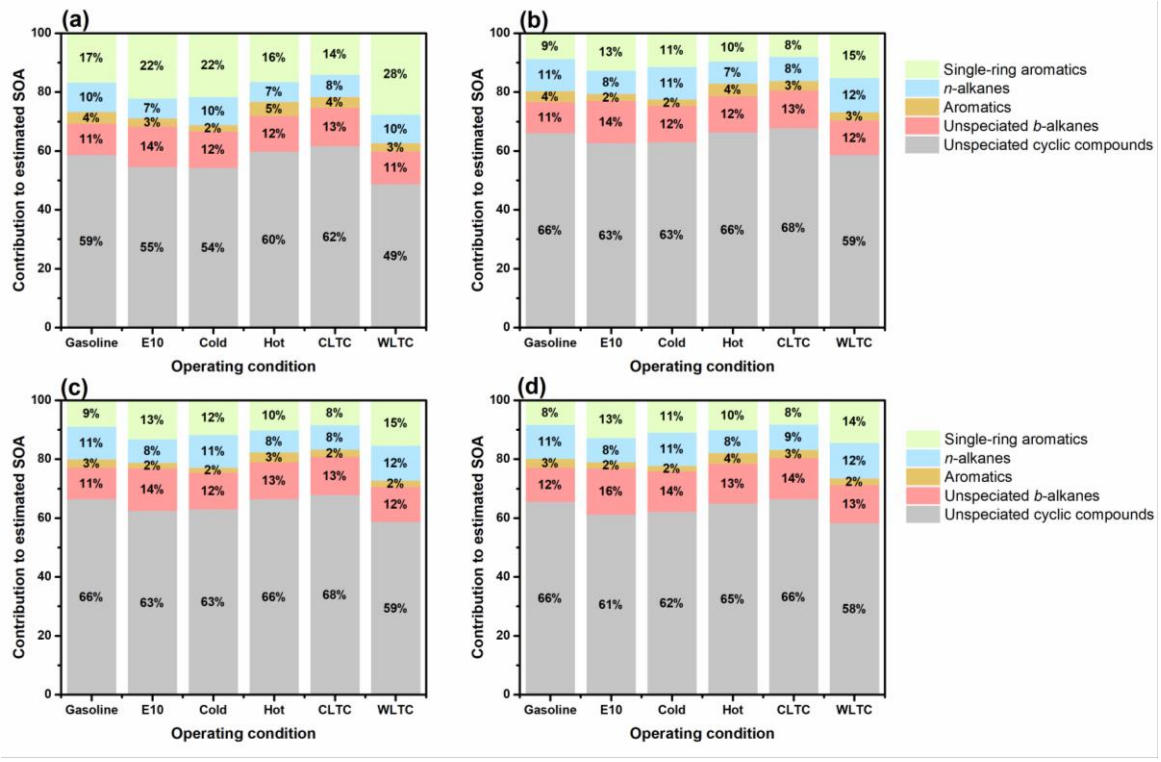

Figure S11. Comparison of the contribution to SOA formation by different chemical compositions, including single-ring VOCs and IVOCs. Here the aromatics represent the PAHs listed in Table S4.

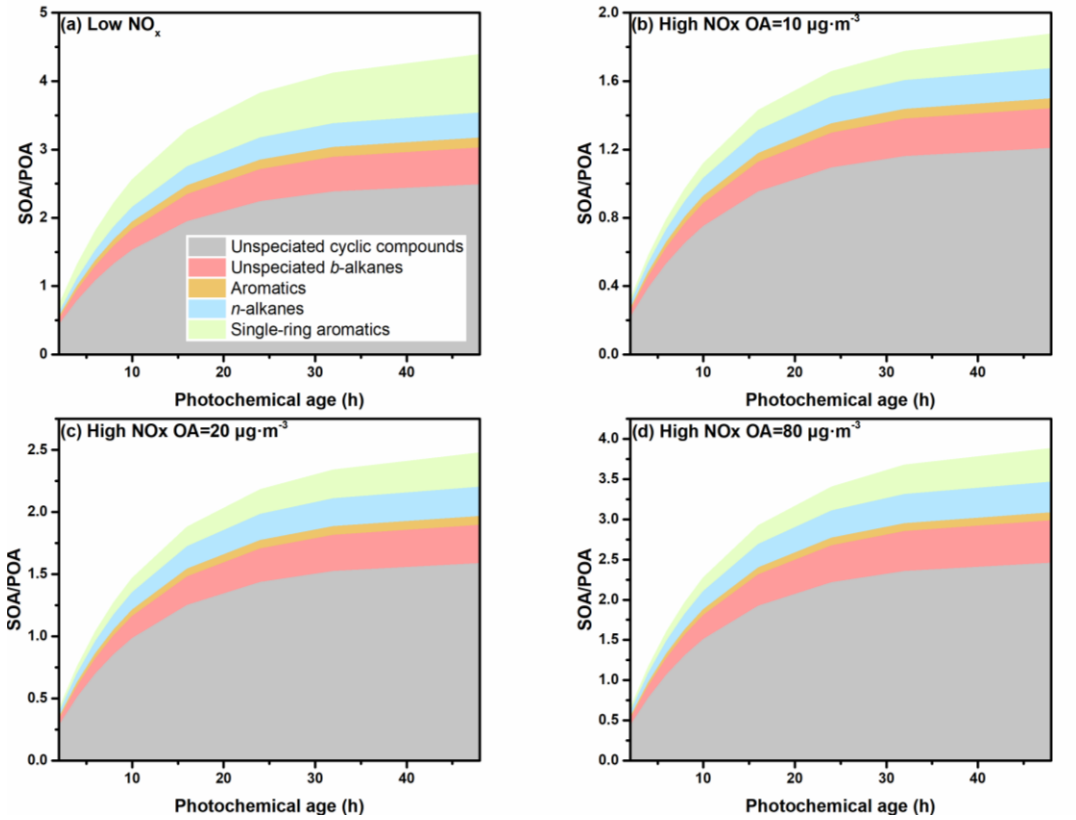

Figure S12. Comparison of the contribution to SOA formation by different chemical compositions, including single-ring VOCs and IVOCs: (a) low NO_x condition; (b) at an OA loading of 10 $\mu g \cdot m^{-3}$

under high NO_x condition; (c) at an OA loading of 20 μg·m^{-3} under high NO_x condition; (d) at an OA loading of 80 μg·m^{-3} under high NO_x condition.

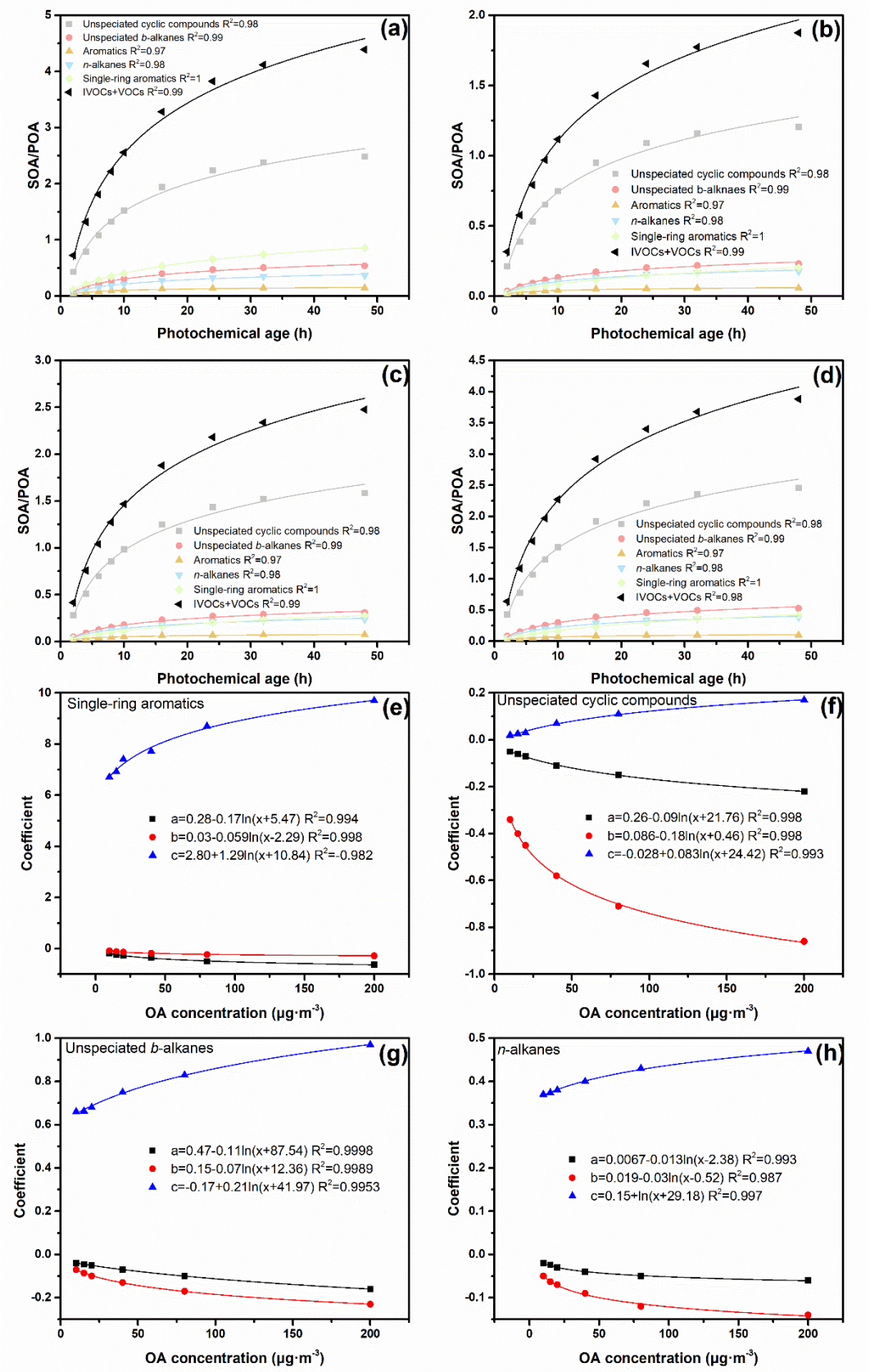

Figure S13. Fits of SOA/POA versus photochemical age at different NOx condition (a)-(d): (a) low NO_x condition; (b) at an OA loading of 10 μg·m^{-3} under high NO_x condition; (c) at an OA loading of 20 μg·m^{-3} under high NO_x condition; (d) at an OA loading of 80 μg·m^{-3} under high NO_x condition. Fits of coefficients (e)-(h): (e) single ring aromatics; (f) unspeciated cyclic compounds; (g) unspeciated *b*-alkanes and (h) *n*-alkanes.

Table S1. The calibration compounds used in this study

Name	Retention time	R^2
Naphthalene-d8	16.843	
Naphthalene	16.93	0.99949
Acenaphthene-d10	24.85	
Acenaphthene	24.993	0.999436
Acenaphthylene	24.145	0.999289
2-Methylnaphthalene	20.129	0.989588
1-Methylnaphthalene	20.545	0.980587
1,4-Dimethylnaphthalene	23.902	0.999524
Phenanthrene-d10	31.673	
Phenanthrene	31.779	0.998865
Anthracene	32.011	0.995482
Fluorene	27.406	0.932439
Fluoranthene	37.279	0.978092
Pyrene	38.245	0.977327
Chrysene-d12	43.966	
Benz(a)anthracene	43.933	0.998571
Chrysene	44.074	0.998533
Perylene-d12	50.046	
Benzo(b)fluoranthene	48.58	0.998833
Benzo(k)fluoranthene	48.691	0.997682
Benzo(a)pyrene	49.806	0.996461
Dibenz(a,h)anthracene	54.503	0.990335
Indeno(1,2,3-cd)pyrene	53.881	0.989301
Benzo(g,h,i)perylene	54.703	0.995117
n-Dodecane-D26	16.979	
n-nonane	8.845	0.989794
n-Decane	11.549	0.998578
n-Undecane	14.495	0.999511
n-Dodecane	17.498	0.99785
n-Tridecane	20.328	0.994602
n-Hexadecane-D34	27.324	
n-Tetradecane	23.017	0.999821
n-Pentadecane	25.523	0.999981
n-Hexadecane	27.892	0.999897

n-Heptadecane	30.153	0.998814
Pristane	30.236	0.978048
n-Eicosane-D42	35.646	
n-Octadecane	32.284	0.996472
Phytane	32.407	0.991827
n-Nonadecane	34.319	0.986211
n-Eicosane	36.266	0.997022
n-Tetracosane-D50	42.596	
n-Heneicosane	38.126	0.999801
n-Docosane	39.906	0.999822
n-Tricosane	41.61	0.999767
n-Tetracosane	43.247	0.99957
n-Pentacosane	44.822	0.999071
n-Hexacosane	46.341	0.998805
n-Triacontane-D62	51.215	
n-Heptacosane	47.808	0.999798
n-Octacosane	49.221	0.99968
n-Nonacosane	50.585	0.999368
n-Dotriacontane-D66	53.718	
n-Triacontane	51.907	0.999498
n-Hentriacontane	53.185	0.999478
n-Dotriacontane	54.421	0.998975
n-Tritriacontane	55.626	0.998547
n-Tetratriacontane	56.792	0.997054
n-Hexatriacontane-D74	58.302	
n-Pentatriacontane	57.933	0.999103
n-Hexatriacontane	59.032	0.997554
n-Heptatriacontane	60.145	0.993378
n-Octatriacontane	61.381	0.990468
n-Tetracontane	64.493	0.97258

Table S2. Key characteristics of driving cycles

Index	**WLTC**	**CLTC**	**UC**
Average velocity (km/h)	46.5	29.0	39.6
Average acceleration (m/s^2)	0.477	0.415	0.673
Average deceleration (m/s^2)	-0.514	-0.464	-0.754
Percentage of idling time	12.2%	22.4%	16.3%

Table S3 Median volatility distribution of IVOCs, SVOCs obtained by GC-MS analysis of Tenax tubes, C* 100 to 106 μg·m-3) as a function of effective saturation concentration (C*, μg·m-3) at 298 K.

Log (C*)	50^{th}
0	0.009
1	0.019
2	0.018
3	0.027
4	0.095
5	0.206
6	0.624

Table S4. List of individual n-alkanes and PAHs and their relative standard deviation (RSD, %)

Compounds	RSD (%)	Compounds	RSD (%)
Naphthalene*	7.8%	*n*-Dodecane*	4.8%
Acenaphthene*	3.2%	*n*-Tridecane*	5.8%
Acenaphthylene*	21.1%	*n*-Tetradecane*	2.0%
2-Methylnaphthalene*	4.4%	*n*-Pentadecane*	3.2%
1-Methylnaphthalene*	2.0%	*n*-Hexadecane*	3.6%
1,4-Dimethylnaphthalene*	5.8%	*n*-Heptadecane*	5.4%
Phenanthrene*	6.7%	*n*-Octadecane*	3.0%
Anthracene*	4.9%	*n*-Nonadecane*	2.0%
Fluorene*	21.3%	*n*-Eicosane*	2.6%
Fluoranthene*	30.6%	*n*-Heneicosane*	5.3%
Pristane*	5.4%	*n*-Docosane*	6.0%
Phytane*	7.1%		

Table S5. OH reaction rate constants（$cm^3 \cdot molec^{-1} \cdot s^{-1}$）and SOA yields for speciated IVOCs included in the SOA model under different NO_x conditions

Name	OH reaction rate	SOA yield Low NO_x	SOA yield High NO_x 10 $\mu g \cdot m^{-3}$	SOA yield High NO_x 20 $\mu g \cdot m^{-3}$	SOA yield High NO_x 80 $\mu g \cdot m^{-3}$
Dodecane	1.32E-11	0.35	0.09	0.12	0.24
Tridecane	1.51E-11	0.44	0.22	0.30	0.52
Tetradecane	1.58E-11	0.54	0.30	0.40	0.62
Pentadecane	1.82E-11	0.63	0.35	0.46	0.67
Hexadecane	1.96E-11	0.78	0.40	0.51	0.70
Heptadecane	2.10E-11	0.88	0.44	0.55	0.73
Octadecane	2.24E-11	0.88	0.44	0.55	0.73
Nonadecane	2.38E-11	0.88	0.44	0.55	0.73
Eicosane	2.52E-11	0.88	0.44	0.55	0.73
Heneicosane	2.67E-11	0.88	0.44	0.55	0.73
Docosane	2.81E-11	0.88	0.44	0.55	0.73
Naphthalene	2.30E-11	0.73	0.21	0.27	0.45
2-methylnaphthalene	4.86E-11	0.58	0.31	0.40	0.50
1-methylnaphthalene	4.09E-11	0.68	0.26	0.34	0.45
Acenaphthylene	1.24E-10	0.31	0.31	0.31	0.31
Acenaphthene	8.00E-11	0.31	0.31	0.31	0.31
Fluorene	1.60E-11	0.31	0.31	0.31	0.31
Phenanthrene	3.20E-11	0.31	0.31	0.31	0.31
Anthracene	1.78E-10	0.31	0.31	0.31	0.31
Fluoranthene	3.30E-11	0.31	0.31	0.31	0.31
Pyrene	5.60E-11	0.31	0.31	0.31	0.31

Table S6. OH reaction rate constants ($cm^3 \cdot molec^{-1} \cdot s^{-1}$) and SOA yields for single-ring aromatics compounds included in SOA model under different NO_x condition.

Name	OH rate constant	SOA yield Low NO_x	SOA yield High NO_x 10 $\mu g \cdot m^{-3}$	SOA yield High NO_x 20 $\mu g \cdot m^{-3}$	SOA yield High NO_x 80 $\mu g \cdot m^{-3}$
Benzene	1.22E-12	0.37	0.14	0.21	0.44
Toluene	5.63E-12	0.30	0.08	0.11	0.15
o-xylene	1.36E-11	0.36	0.05	0.06	0.09
m/p-xylene	1.87E-11	0.36	0.05	0.06	0.09
Ethylbenzene	7.00E-12	0.30	0.08	0.11	0.15
Styrene	5.80E-11	0.30	0.08	0.11	0.15
isopropylbenzene	6.3E-12	0.30	0.08	0.11	0.15
n-propylbenzene	5.80E-12	0.30	0.08	0.11	0.15
p-ethyl-toluene	1.18E-12	0.30	0.08	0.11	0.15
o-ethyl-toluene	1.19E-11	0.30	0.08	0.11	0.15
m-ethyl-toluene	1.86E-11	0.30	0.08	0.11	0.15
1,3,5-trimethyl-benzene	5.67E-11	0.36	0.05	0.06	0.09
1,2,4-trimethyl-benzene	3.25E-11	0.36	0.05	0.06	0.09
1,2,3-trimethyl-benzene	3.27E-11	0.36	0.05	0.06	0.09

Table S7. Surrogate compounds (n-alkanes) used for OH reaction rate constants ($cm^3 \cdot molec^{-1} \cdot s^{-1}$) and SOA yields for unspeciated cyclic compounds

Bins	OH rate constant	Surrogate compounds for SOA yields	
		Unspeciated cyclic compounds	Unspeciated cyclic compounds
B12	C12	C10	C12
B13	C13	C11	C13
B14	C14	C12	C14
B15	C15	C13	C15
B16	C16	C14	C16
B17	C17	C15	C17
B18	C18	C16	C18
B19	C19	C17	C19
B20	C20	C18	C20
B21	C21	C19	C21
B22	C22	C20	C22

References

Huang, G., Liu, Y., Shao, M., Li, Y., Chen, Q., Zheng, Y., Wu, Z., Liu, Y., Wu, Y., Hu, M., Li, X., Lu, S., Wang, C., Liu, J., Zheng, M., and Zhu, T.: Potentially Important Contribution of Gas-Phase Oxidation of Naphthalene and Methylnaphthalene to Secondary Organic Aerosol during Haze Events in Beijing, Environmental Science & Technology, 53, 1235-1244, 10.1021/acs.est.8b04523, 2019.

Tutuianu, M., Bonnel, P., Ciuffo, B., Haniu, T., Ichikawa, N., Marotta, A., Pavlovic, J., and Steven, H.: Development of the World-wide harmonized Light duty Test Cycle (WLTC) and a possible pathway for its introduction in the European legislation, Transportation Research Part D: Transport and Environment, 40, 61-75, https://doi.org/10.1016/j.trd.2015.07.011, 2015.

Zhao, Y., Nguyen, N. T., Presto, A. A., Hennigan, C. J., May, A. A., and Robinson, A. L.: Intermediate Volatility Organic Compound Emissions from On-Road Gasoline Vehicles and Small Off-Road Gasoline Engines, Environmental Science & Technology, 50, 4554-4563, 10.1021/acs.est.5b06247, 2016.